
Evidential Sparsification of Multimodal Latent Spaces in Conditional Variational Autoencoders

Masha Itkina, Boris Ivanovic, Ransalu Senanayake, Mykel J. Kochenderfer, Marco Pavone

Department of Aeronautics and Astronautics

Stanford University

{mitkina, borisi, ransalu, mykel, pavone}@stanford.edu

Abstract

Discrete latent spaces in variational autoencoders have been shown to effectively capture the data distribution for many real-world problems such as natural language understanding, human intent prediction, and visual scene representation. However, discrete latent spaces need to be sufficiently large to capture the complexities of real-world data, rendering downstream tasks computationally challenging. For instance, performing motion planning in a high-dimensional latent representation of the environment could be intractable. We consider the problem of sparsifying the discrete latent space of a trained conditional variational autoencoder, while preserving its learned multimodality. As a post hoc latent space reduction technique, we use *evidential theory* to identify the latent classes that receive direct evidence from a particular input condition and filter out those that do not. Experiments on diverse tasks, such as image generation and human behavior prediction, demonstrate the effectiveness of our proposed technique at reducing the discrete latent sample space size of a model while maintaining its learned multimodality.

1 Introduction

Variational autoencoders (VAEs) with discrete latent spaces have recently shown great success in real-world applications, such as natural language processing [1], image generation [2, 3], and human intent prediction [4]. Discrete latent spaces naturally lend themselves to the representation of discrete concepts such as words, semantic objects in images, and human behaviors. The choice of a discrete latent space encoding over a continuous one has also been shown to encourage multimodal predictions [5, 6] as well as interpretability [7, 8] since it is easier to analyze input-output relationships on countable classes than continuous vector spaces [9]. However, prohibitively large discrete latent spaces are required to accurately learn complex data distributions [10, 11], thereby causing difficulties in interpretability and rendering downstream tasks computationally challenging. For instance, robotic motion planning algorithms often plan using a uniform distribution over the state space representation, requiring exorbitantly many samples to accurately cover a large latent space [12]. Similarly, in multi-agent robotics, a high dimensional latent space encoding may be too large to transmit over limited bandwidth between coordinating robots [13]. In an attempt to address these concerns, we propose a methodology that effectively reduces the latent sample space size while maintaining multimodality within the latent distribution.

Distributional multimodality arises in many real-world problems, such as video frame prediction [14] and human behavior prediction [8, 15], from multiple possibilities for the future (e.g., a pedestrian may turn right or left given the same trajectory history). The conditional variational autoencoder (CVAE) was developed to address prediction multimodality [16]. The CVAE encodes input data x and corresponding query label y into a latent space Z . At test time, the model samples from the latent space encoding of a query label to generate diverse data. The latent space distribution $p(z | y)$

encodes the multimodality of the prediction task. During inference, the discrete latent distribution in a CVAE is often parameterized by the softmax function. A drawback to the softmax transformation is that uncertainty is distributed across all the available classes since, by definition, the softmax function cannot set a probability to zero (though it can become negligible). Removing latent classes that arise within the distribution solely due to this uncertainty has the potential to reduce the number of relevant latent classes to consider.

Contributions We introduce a novel method grounded in evidential theory for sparsifying the discrete latent space of a trained CVAE. Evidential theory, also known as Dempster-Shafer Theory (DST), differentiates lack of information (e.g., an uninformative prior) from conflicting information (e.g., evidence supporting multiple hypotheses) by considering the power set of hypotheses [17]. We propose using evidential conflict as a proxy for multimodality. We can then prune the latent classes from the distribution that do not directly receive evidence from the input features, thus performing post hoc latent space sparsification without sacrificing distributional multimodality. Experiments show that our algorithm achieves a significant reduction in the discrete latent sample space of CVAE networks trained for the tasks of image generation and behavior prediction, without loss of network performance. Our approach sparsifies the latent space while maintaining distributional multimodality, unlike baseline techniques which remove important modes with overly aggressive filtering. Our proposed method provides a more accurate distribution over the latent encoding with fewer training iterations than baseline methods, and demonstrates consistent performance on downstream tasks.

2 Evidential Theory for Latent Space Reduction

Evidential theory distinguishes lack of information from conflicting information [17], making it appealing for handling epistemic uncertainty in machine learning tasks [18]. Denoeux [19] recently showed that, under a set of assumptions, the softmax transformation is equivalent to the Dempster-Shafer fusion of belief masses. This insight facilitates the use of evidential theory in multi-class machine learning classification paradigms. We propose using the tools from evidential theory to sparsify discrete latent spaces in CVAEs. Our method automatically balances the objectives of sparsity and multimodality by keeping only the latent classes that receive direct evidence from the network’s features and weights. The following sections overview evidential theory, its application to neural network classifiers, and our proposed approach to evidential latent space sparsification in CVAEs. Further information on evidential theory can be found in Appendix A.

2.1 Evidential Theory

Mass Functions Evidential theory considers a discrete set of hypotheses or, equivalently, classes. Let the set of allowable classes be $Z = \{z_1, \dots, z_K\}$, where z_k can be represented as one-hot encodings, and denote its power set by 2^Z . A belief mass is a function $m : 2^Z \rightarrow [0, 1]$ such that $\sum_{A \subseteq Z} m(A) = 1$ [17]. Evidential theory assumes that the allowable classes are exhaustive, that is $m(\emptyset) = 0$ [20]. The mass function quantifies the total evidential belief committed to some $A \subseteq Z$. If $m(Z) = 1$, then the mass function is vacuous, in that it encodes a complete lack of evidence for any particular subset of classes. If the belief mass function is non-zero only for singleton sets, then it reduces to an approximation of the usual categorical distribution. Two mass functions, each representing an independent source of evidence, can be combined through Dempster’s rule [17] to generate a fused belief mass as defined in Appendix A.3.

A belief mass function m is *simple* if there is at most a single strict subset $A \subset Z$ for which $m(A)$ is non-zero. Then, we can define,

$$m(A) = s, \quad m(Z) = 1 - s, \quad w = -\log(1 - s), \quad (1)$$

where $s \in [0, 1]$ is the degree of support in A and w is the corresponding *evidential weight* for A [20].

Plausibility Transformation Plausibility $pl(z_k)$ represents the extent to which the evidence does not contradict the class z_k [21]. Belief masses can be reduced to estimated probabilities through the plausibility transformation [22],

$$p(z_k) = \frac{pl(z_k)}{\sum_{l=1}^K pl(z_l)}, \quad (2)$$

where $pl(z_k) = \sum_{B: z_k \in B, B \subseteq Z} m(B)$ and $k \in \{1, \dots, K\}$.

2.2 Evidential Classifiers

It has been shown that all classifiers that transform a linear combination of features through the softmax function can be formulated as evidential classifiers [19]. Each feature represents an elementary piece of evidence in support of a class or its complement. The softmax function then fuses these pieces of evidence to form class probabilities conditioned on the input. In this context, the softmax class probabilities are equivalent to normalized plausibilities (Eq. (2)). Thus, the neural network weights and features, which serve as arguments to the softmax function, can also be used to compute the corresponding belief mass function. When compared to a Bayesian probability distribution, a belief mass function provides an additional degree of freedom that allows it to distinguish between a lack of evidence and conflicting evidence.

A feature vector $\phi(y_i) \in \mathbb{R}^J$ is defined as the output of the last hidden layer in a neural network, for a given query y_i from a dataset. The evidential weights defined in Eq. (1) are assumed to be affine transformations of each feature $\phi_j(y_i)$ by construction,

$$w_{jk} = \beta_{jk}\phi_j(y_i) + \alpha_{jk}, \quad (3)$$

where α_{jk} and β_{jk} are parameters [19]. An assumption is made that the evidence supports at most either a singleton class $\{z_k\}$ when $w_{jk}^+ = \max(0, w_{jk}) > 0$ or its complement $\{\overline{z_k}\}$ when $w_{jk}^- = \max(0, -w_{jk}) > 0$, such that $w_{jk}^+ - w_{jk}^- = w_{jk}$. Then, for each feature $\phi_j(y_i)$ and each class z_k , according to Eq. (1), there exist two simple mass functions,

$$m_{kj}^+(\{z_k\}) = 1 - e^{-w_{jk}^+}, \quad m_{kj}^+(Z) = e^{-w_{jk}^+} \quad (4)$$

$$m_{kj}^-(\{\overline{z_k}\}) = 1 - e^{-w_{jk}^-}, \quad m_{kj}^-(Z) = e^{-w_{jk}^-}. \quad (5)$$

These masses can then be fused through Dempster's rule to arrive at the mass function at the output of the softmax layer as follows,

$$m(\{z_k\}) = C e^{-w_k^-} \left(e^{w_k^+} - 1 + \prod_{\ell \neq k} (1 - e^{-w_\ell^-}) \right) \quad (6a)$$

$$m(A) = C \left(\prod_{z_k \notin A} (1 - e^{-w_k^-}) \right) \left(\prod_{z_k \in A} e^{-w_k^-} \right), \quad (6b)$$

where $A \subseteq Z$, $|A| > 1$, C is a normalization constant, $w_k^- = \sum_{j=1}^J w_{jk}^-$, and $w_k^+ = \sum_{j=1}^J w_{jk}^+$.

2.3 Evidential Sparsification

Under the assumptions outlined in Section 2.2 and using the plausibility transformation, the equivalence of the mass function in Eq. (6) and the softmax distribution holds under the constraint $\sum_{j=1}^J \alpha_{jk} = \hat{\beta}_{0k} + c_0$, where $\hat{\beta}_{0k}$ are the bias parameters learned by the neural network and c_0 is a constant [19]. The evidential weight parameters α_{jk} and β_{jk} in Eq. (3) are not uniquely defined due to the extra degree of freedom provided by the belief mass as compared to the softmax distribution. Denoeux [19] selects the α_{jk} and β_{jk} parameters that maximize the Least Commitment Principle (LCP), which is analogous to maximum entropy in information theory [23].

In contrast, we choose our parameters such that the singleton mass function in Eq. (6a) is sparse, rather than distributing uncertainty across the mass function using the LCP. We construct the singleton mass function to identify only the classes that receive direct evidence towards them. We observe that if $w_k^+ = 0$ and $w_\ell^- = 0$ for at least one other class $\ell \neq k$, then $m(\{z_k\}) = 0$. Intuitively, if no evidence directly supports class k and there is no evidence contradicting another class ℓ , then the belief mass for the singleton set $\{z_k\}$ is zero. This situation occurs when at least one of w_k^+ and w_k^- is zero, which holds if $w_k^+ = \max(0, w_k)$ and $w_k^- = \max(0, -w_k)$, where $w_k = \sum_{j=1}^J w_{jk}$. Hence, w_k provides direct support either for or against a class k . This property does not hold in the original formulation by Denoeux [19]. Thus, we construct an evidential weight w_{jk} that does not depend on j , enforcing this desideratum:

$$w_{jk} = \frac{1}{J} \left(\beta_{0k} + \sum_{j=1}^J \beta_{jk} \phi_j(y_i) \right). \quad (7)$$

Since w_{jk} is constant across the index j , summing over j in w_{jk}^+ and w_{jk}^- yields $w_k^+ = \max(0, w_k)$ and $w_k^- = \max(0, -w_k)$, as required. The corresponding parameters in Eq. (3) are then:

$$\beta_{jk} = \hat{\beta}_{jk} - \frac{1}{K} \sum_{l=1}^K \hat{\beta}_{jl} \quad (8)$$

$$\alpha_{jk}(y_i) = \frac{1}{J} \left(\beta_{0k} + \sum_{j=1}^J \beta_{jk} \phi_j(y_i) \right) - \beta_{jk} \phi_j(y_i), \quad (9)$$

where $\hat{\beta}_{jk}$ are the output linear layer weights learned by the neural network a priori. These parameters match those of Denoeux [19], except $\phi_j(y_i)$ replaces $\mu_j = \frac{1}{N} \sum_{i=1}^N \phi_j(y_i)$ in α_{jk} . The α_{jk} bias term is now a function of the test input query y_i . By choosing to treat each input y_i individually at test time, we remove the dependency in w_{jk} on j , facilitating our desired behavior in the singleton mass function. We show that the new α_{jk} and β_{jk} parameters satisfy the constraint to achieve equivalency with the softmax transformation in Appendix B. We posit that filtering out the classes with zero singleton belief mass values according to the proposed definition removes only the classes without direct evidence in their support, while imposing a more concentrated distribution output.

2.4 Post Hoc CVAE Latent Space Sparsification

Since the discrete latent distribution in a CVAE is parameterized using a softmax function at test time, we can directly apply the evidential theory formulation developed in Sections 2.1–2.3 to sparsify the latent space of a trained CVAE. The evidence allocated to multiple singleton latent classes indicates *internal conflict* between them within the mass function. In the context of a CVAE, we posit that internal conflict is directly correlated with latent space multimodality. High evidential conflict between a subset of latent classes indicates distinct, multimodal latent features encoded by the network. We propose filtering the latent distribution to maintain only these highly conflicting classes, thus, reducing latent sample space dimensionality, without compromising the captured multimodality.

Using Eq. (6a) and Eq. (7), we construct the singleton mass function that corresponds to the encoder’s output softmax distribution $p(z | y)$ over the latent classes z_k given an input query y . This distribution is filtered by removing the probabilities for the latent classes with zero singleton mass values and then renormalizing, as follows,

$$p_{\text{filtered}}(z_k | y) = \frac{\mathbb{1}\{m(\{z_k\}) \neq 0\} p_{\text{softmax}}(z_k | y)}{\sum_{\ell=1}^K \mathbb{1}\{m(\{z_\ell\}) \neq 0\} p_{\text{softmax}}(z_\ell | y)}. \quad (10)$$

In this manner, we reduce the number of relevant latent classes, providing a more concentrated latent class distribution, while maintaining the learned distributional multimodality.

3 Experiments

To validate our method, we consider CVAE architectures designed for the tasks of class-conditioned image generation and pedestrian trajectory prediction. These real-world tasks require modeling high degrees of distributional multimodality. We compare our method to the softmax distribution and the popular class-reduction technique termed *sparsemax* which achieves a sparse distribution by projecting an input vector onto the probability simplex [24]. By design, both our method and *sparsemax* compute an implicit threshold for each input query post hoc. Thus, they do not need to be tuned for each network or dataset, and automatically adapt to individual input features. Experiments indicate that our method is able to better balance the objectives of sparsity and multimodality than *sparsemax* by keeping only the latent classes that receive direct evidence from the network’s features and weights, as described in Section 2. We demonstrate that our method maintains distributional multimodality, unlike *sparsemax*, whilst yielding a significantly reduced latent sample space size over softmax. The code to reproduce our results can be found at: <https://github.com/sisl/EvidentialSparsification>.

3.1 Image Generation

To gain insight into our proposed approach, we run experiments on a small network trained on MNIST [25]. We then demonstrate the performance of our sparsification algorithm on the large

discrete latent space within the state-of-the-art VQ-VAE [2] architecture trained on *miniImageNet* [26]. All image generation experiments were run on a single NVIDIA GeForce GTX 1070 GPU.

3.1.1 MNIST Experiments

Task To investigate discrete, multimodal latent representations, we consider the multimodal task of generating digit images for *even* and *odd* queries ($y \in \{\text{even}, \text{odd}\}$) on MNIST. Appendix F and Appendix G contain results on Fashion MNIST [27] and NotMNIST [28], respectively.

Model We present a proof of concept of our method for sparsifying multimodal discrete latent spaces on the CVAE architecture shown in Fig. 1. We intentionally use a simplistic CVAE architecture trained on a reasonably simple task to 1) demonstrate the capability of our latent space reduction technique to improve performance post hoc and 2) easily characterize the results.

During training, the encoder consists of two multi-layer perceptrons (MLPs). One MLP takes as input the query y , and outputs a softmax distribution that parameterizes the categorical prior distribution $p(z | y)$ over the latent variable z . The other MLP takes as input a feature vector x and the query y , and outputs the softmax distribution for the posterior $q(z | x, y)$. The latent class is sampled from q during training and p at test time. It is then passed through the decoder MLP to generate the feature vector x' . The Gumbel-Softmax distribution is used to backpropagate gradients through the discrete latent space [7, 29]. The model is trained to maximize the standard conditional evidence lower bound (ELBO) [16]. Further experimental details are provided in Appendix C.

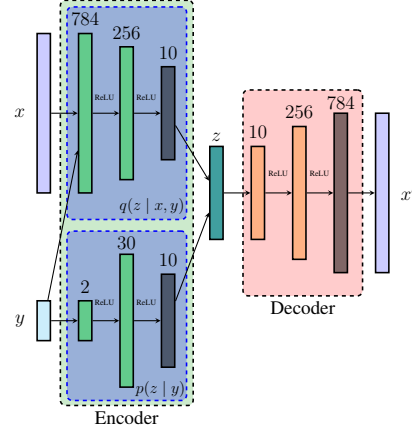


Figure 1: The CVAE architecture used for MNIST image generation. The last layer in each MLP is a softmax layer. At test time, $p(z | y)$ is used to sample the latent space.

Qualitative Performance We choose $K = 10$ latent classes; with a “perfectly trained” network, this would yield a 5-modal distribution when conditioned on one of $y \in \{\text{even}, \text{odd}\}$. For instance, conditioning on the *even* query should produce a uniform distribution over the encoded digits: 0, 2, 4, 6, and 8. Fig. 2 depicts the latent distributions of our proposed method, softmax, and sparsemax for the *even* and *odd* queries. Although the CVAE in Fig. 1 successfully learns a multimodal latent encoding, the learned softmax distribution has non-negligible probability mass associated with the incorrect latent classes z_k for each query class y . Thus, sampling from the CVAE with the softmax distribution results in an imperfect set of generated digit images given a query as shown in Appendix D.

To remedy this problem, we consider both sparsemax and our proposed evidential filtration technique. In Fig. 2, our filtered distribution selects an almost perfect set of correct latent classes given a query. The proposed distribution provides a more robust signal to the decoder network, improving the accuracy of the sampled images as demonstrated in Appendix D. Thus, we successfully sparsify the

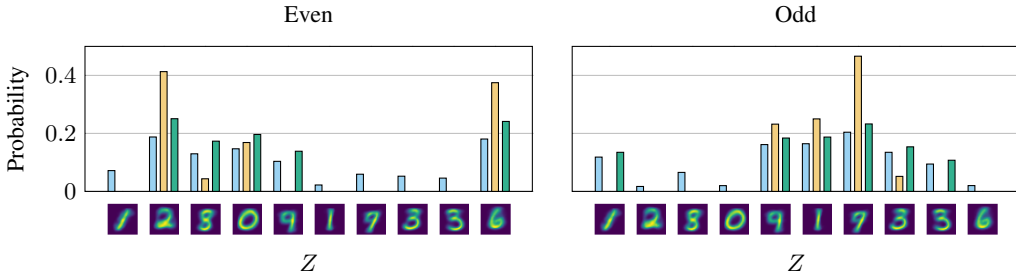


Figure 2: Our proposed filtered distribution (green) yields a more accurate distribution on the MNIST dataset than softmax (blue) and sparsemax (orange). Our method reduces the size of the relevant latent sample space without removing valid latent classes. The horizontal axis depicts the decoded image for each latent class.

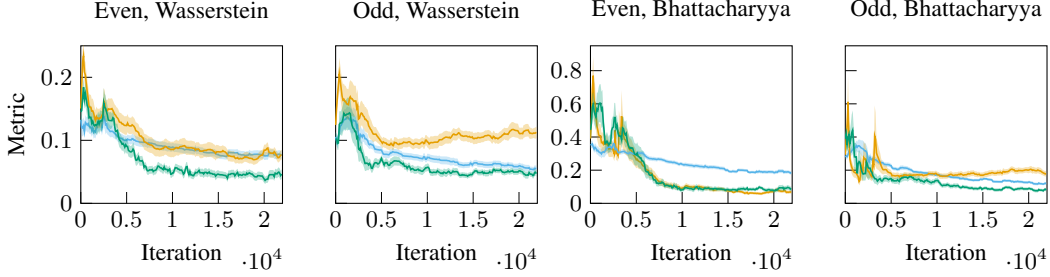


Figure 3: Our filtered distribution (green) outperforms the softmax (blue) and sparsemax (orange) baselines across training iterations on the MNIST dataset. Lower is better.

latent space analytically for each query without knowledge of or comparison to the other query. The only error made by the filtered distribution is the selection of the 9 image (fifth latent class) for the *even* query. This error can be explained by the relatively high softmax probability assigned to the 9 image for both the *even* and *odd* queries. The key insight to our approach is that it performs only as well as the quality of the representation learned by the neural network, with the benefit of extracting richer information than softmax. In contrast, sparsemax results in undesirably more aggressive filtering than our method. It removes the correct latent classes of 1 and 3 for the *odd* query. Both our method and sparsemax result in a filtration decision through an implicit thresholding of the softmax distribution internal to each individual method. Our filtration technique based in evidential theory results in an empirically lower implicit threshold than that of sparsemax. Thus, our more conservative filtration is a compelling latent space reduction technique, particularly for applications where false negatives might cause safety concerns. One such application is human behavior prediction in the context of autonomous driving, which we consider in Section 3.2.

As a further thought experiment, we consider a static threshold that could be chosen through hyperparameter tuning on a validation set. By visual inspection, it is impossible to choose a single static threshold that would outperform our method in balancing sparsity and multimodality in Fig. 2 (either additional false negatives or false positives would result). While we could tune a static threshold for each individual input query for the MNIST task, this would be intractable for a continuous trajectory input query as in the behavior prediction task in Section 3.2.

Quantitative Evaluation Metrics Quantitatively evaluating the performance of the filtered distribution is nontrivial as the ground truth distribution can be ambiguous (e.g., a generated image may look like a 3 or an 8). To standardize the evaluation for this binary-input task, we introduce the following metric. The target probability for an input is set to zero if the learned softmax probability conditioned on the input $p(z_k | y)$ is smaller than its complement $p(z_k | \bar{y})$. If it is larger, then the target probability takes the value of $p(z_k | y)$. The result is then normalized across latent classes. Thus, we obtain a sparse, multimodal distribution over the more prominent classes as learned by the network. We write the target distribution as $p_T(z_k | y) = \frac{\mathbb{1}\{p(z_k | y) \geq p(z_k | \bar{y})\} p(z_k | y)}{\sum_{\ell=1}^K \mathbb{1}\{p(z_\ell | y) \geq p(z_\ell | \bar{y})\} p(z_\ell | y)}$. We use the Wasserstein and Bhattacharyya distances to the target distribution as evaluation metrics. The Kullback-Leibler divergence is not used as it is undefined for zero probabilities.

Training Iteration Evolution Fig. 3 demonstrates the robustness of the filtered distribution to fewer training iterations in its ability to extract more accurate encoding information from the neural network earlier in the training process than softmax¹. Our methodology provides significant performance improvement over the softmax baseline when the latter assigns non-negligible probability mass to incorrect latent classes given a query, as is the case for the *even* query as shown in Fig. 2 and Fig. 3. Although the performances of sparsemax and our proposed distributions are similar for the *even* query on the Bhattacharyya metric, sparsemax significantly underperforms for the *odd* query, even as compared to softmax. The aggressive filtration within sparsemax incorrectly filters out potentially valid latent classes for the *odd* query. Thus, our method consistently outperforms both baselines on MNIST, on average resulting in a 22% improvement over softmax and a 10% improvement over sparsemax on the Bhattacharyya metric. Thus, the proposed latent distribution provides a more robust

¹The results are over 25 different random seeds.

Table 1: Downstream classification performance on 1600 sampled images (25 samples \times 64 classes) shows that our sparse distribution maintains the original softmax performance, unlike sparsemax. For comparison, the classifier was evaluated on a held-out subset of 1920 images from the original *miniImageNet* training set. Higher is better for all metrics and bold highlights the best performing latent distributions.

	Softmax	Sparsemax	Ours	Original Images
Accuracy (%)	20.688	6.125	19.937	71.719
Top 5 Class Accuracy (%)	47.750	17.500	47.875	90.625

representation, retrieving richer information from the learned neural network weights with fewer training iterations. We present further experiments on a reduced data model in Appendix E.

3.1.2 VQ-VAE Experiments

We demonstrate the performance of our sparsification methodology on a much larger latent sample space within the state-of-the-art VQ-VAE [2] image generation architecture. The VQ-VAE architecture is trained in two stages. First, the encoder-decoder is trained assuming a uniform prior over the discrete latent space. Then an autoregressive prior is trained over the latent space to allow for sampling from the network. We use *miniImageNet* images randomly cropped to 128×128 pixels for training as opposed to ImageNet [30] due to limited computational resources. We consider a latent space of 32×32 discrete latent variables with $K = 512$ classes each. As in the original paper [2], we train a PixelCNN [31] network for the prior, but reduce its capacity to 20 layers with a hidden dimension size of 128. Further experimental details can be found in Appendix H².

Our algorithm achieves an 89% reduction in the 512 latent classes required to represent each latent variable, while maintaining the multimodality of the distribution. On the other hand, sparsemax achieves a 99% reduction in the latent sample space, but sacrifices multimodality, resulting in degenerate single color images sampled from the autoregressive prior. Although sparsemax reduces the latent sample space by a larger percentage than our technique, this negatively impacts its performance due to undesirable pruning of correct latent classes. To further evaluate the performance of our proposed sparse latent distribution, we consider the downstream task of image classification. We train a Wide Residual Network (WRN) [32] for classification on the *miniImageNet* data. We generate a dataset of 25 examples from each of the 64 training classes in *miniImageNet* by sampling from the prior. The decoded images are then classified by the WRN. Table 1 shows that our much smaller latent space successfully maintains the performance of the original softmax distribution.

3.2 Behavior Prediction

We show that our sparse latent sample space allows for easier interpretability and maintains distributional multimodality on the difficult task of pedestrian trajectory prediction. Trajectron++ [4] is a state-of-the-art deep probabilistic generative model of pedestrian trajectories. It is a graph-structured recurrent model that produces a distribution over future trajectories given an agent’s past trajectory history and the past trajectories of its neighboring agents. The model uses a CVAE to capture the multimodality over future trajectory predictions, with a latent space comprised of two discrete variables with five classes each, resulting in 25 total latent classes. The loss function is comprised of the classic conditional ELBO loss in a β -VAE [33] scheme and a mutual information loss term on z and y as per [34]. We evaluate Trajectron++’s performance with different probability filtering schemes on 203 randomly-sampled examples from the test set of the ETH pedestrian dataset [35], consisting of real world human trajectories with rich interaction scenarios. Behavior prediction model training and experiments were performed on two NVIDIA GTX 1080 Ti GPUs. Further experimental details are provided in Appendix I.

We demonstrate our method’s performance as compared to the softmax and sparsemax baselines in Fig. 4. Our filtered latent space kept 2 – 12 latent classes out of 25 total (51.7% of the test set resulted in 6 maintained latent classes), achieving more than a 50% reduction. Despite the significant sample space reduction, our filtered distribution successfully captures the ground truth when the learned latent space encompasses it, while maintaining the multimodality of the output as seen in Fig. 4. For instance, in Fig. 4a and Fig. 4c, our method identifies two distinct modes where the pedestrian is

²We largely follow the training procedure here: <https://github.com/ritheshkumar95/pytorch-vqvae/>.

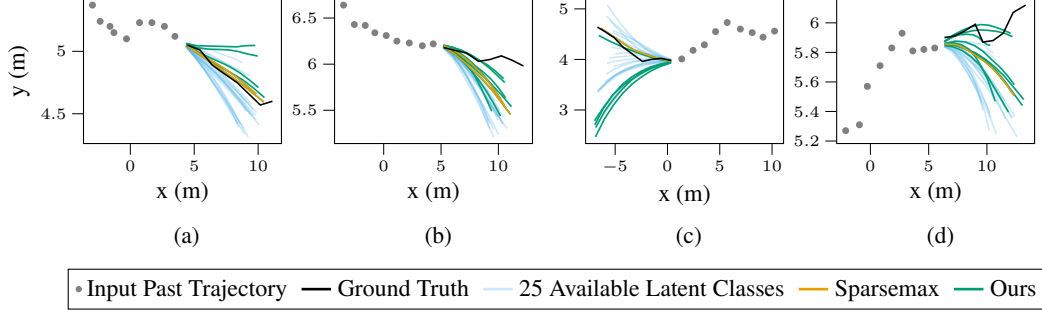


Figure 4: Behavior prediction results on the ETH pedestrian dataset [35] show that our method selects distinct, interpretable modes in the latent space while capturing the ground truth. In contrast, sparsemax occasionally misses the ground truth due to its aggressive filtering scheme. We averaged 100 samples from the Trajectron++’s output for each latent class.

predicted to follow an approximately straight path or choose to turn, both visually valid options. The reduced number of trajectories and the appearance of distinct modes in the filtered output aids with the interpretability of the latent space.

We consider two quantitative experiments in Table 2: 1) sampling from the network according to each of the softmax, sparsemax and our latent distributions and 2) considering the five most likely latent classes according to each distribution and taking the best metric across them. We use standard trajectory prediction metrics to evaluate performance: the Average Displacement Error (ADE), Final Displacement Error (FDE), and Negative Log Likelihood (NLL) [4]. In the sampling experiment, both our proposed distribution and sparsemax quantitatively perform similarly on average to the original softmax distribution, but with the benefit of a significantly reduced latent sample space. However, sampling may not cover a sufficient number of modes due to high likelihoods in a single class. In the second experiment, our method maintains the same performance as softmax, but outperforms sparsemax due to the latter generating false negatives, and collapsing the captured multimodality. As seen qualitatively, although, sparsemax results in a sparser latent distribution, it filters out potentially valid modes as in Fig. 4b and Fig. 4d, reducing its applicability in such safety critical applications as behavior prediction in the context of autonomous driving.

4 Related Work

In recent years, a number of new perspectives on the softmax function have been presented. The Gumbel-Softmax distribution was introduced to allow backpropagation through categorical distributions, giving rise to the popularity of discrete latent spaces within CVAE architectures [7, 29]. Related works in low-dimensional encodings for VAEs generally focus on regularization [36] and enforcing structure in the latent space [37] during training, but they do not sparsify the latent space post hoc. Sensoy et al. [38] present an evidential approach to epistemic uncertainty estimation in neural networks for classification tasks. They propose learning Dirichlet distribution parameters to form a distribution over softmax functions. The Dirichlet parameters serve as evidence towards singleton classes, resulting in a loss that regularizes misleading evidence towards the vacuous mass. Unlike Sensoy et al. [38], we focus on post hoc distributional sparsification rather than capturing epistemic uncertainty. Duch and Itert [39] suggest a post hoc modification to further disperse uncertainty among the classes, thus *flattening* the softmax distribution to improve classification performance. Conversely, we are interested in removing the classes that have probability mass assigned to them due to uncertainty rather than evidence, in this way generating a more *sharply peaked* distribution.

Martins and Astudillo [24] introduce the sparsemax distribution, which follows similar motivations to our work in 1) filtering large output spaces and 2) addressing multimodality in classification tasks. An important distinction between our work and sparsemax is the formulation of the problem to arrive at the sparse distribution. Sparsemax finds the Euclidean projection of the input onto the probability simplex. In contrast, we identify a sparse distribution by means of evidential theory, filtering the classes that do not have direct evidence towards them as determined by the learned weights of the neural network. Empirically, we demonstrate that sparsemax results in undesirably more aggressive filtering than our method, making it less effective for applications where false negatives could result

Table 2: Our proposed distribution maintains performance with softmax, while sparsifying the latent space. It preserves the multimodality of the original distribution, unlike sparsemax, which collapses the multimodality, as seen when computing the minimum over the top five most likely latent modes. Direct sampling metrics were computed over 2000 samples from the Trajectron++ network and the top five metrics were computed over 500 samples per latent class. For all metrics lower is better and the best performance is highlighted in bold.

	Softmax	Sparsemax	Ours
		Direct Sampling	
NLL	4.698 ± 0.443	4.698 ± 0.443	4.686 ± 0.453
ADE	0.558 ± 0.001	0.558 ± 0.001	0.559 ± 0.001
FDE	1.141 ± 0.002	1.141 ± 0.002	1.142 ± 0.002
		Top 5 Sampling	
NLL	3.951 ± 0.425	4.360 ± 0.422	3.862 ± 0.419
ADE	0.376 ± 0.021	0.397 ± 0.021	0.376 ± 0.021
FDE	0.757 ± 0.049	0.802 ± 0.051	0.753 ± 0.050

in a reduction of safety. Laha et al. [40] augment the sparsemax technique to control sparsity, presenting sparsegen-lin (sparsemax with regularization) and sparsegen-hg (sparsemax with a scaled input). Both of these methods require hyperparameter tuning to achieve a sparse distribution post hoc which may be computationally prohibitive on larger networks. Our method is able to automatically balance the objectives of sparsity and multimodality while adapting to different feature inputs without hyperparameter tuning. Concurrently to our work, Correia et al. [41] introduced a sparsemax-based method for backpropagating through a discrete latent space as an alternative to the Gumbel-Softmax relaxation. Correia et al. [41] focus on latent space sparsification to allow for efficient marginalization during training, while our work focuses on post hoc latent space sparsification that preserves the learned multimodality.

5 Conclusions

In this work, we present a fully analytical methodology for post hoc discrete latent space sparsification in CVAEs. The proposed filtered distribution outperforms the ubiquitous softmax and sparsemax distributions in experiments, extracting more accurate information with fewer training iterations, while improving interpretability and significantly reducing the latent sample space size during inference. We leave the investigation of evidential latent space reduction at training time to future work.

Broader Impact

Our work focuses on sparsifying the latent space of a conditional variational autoencoder (CVAE). We consider the tasks of image generation and pedestrian trajectory prediction for empirical evaluation. We intend our work to be applicable in the domain of robotics. For instance, our method has the potential to improve tractability of motion planning in a latent representation of the robot’s dynamics and to decrease the amount of information required to be transmitted between coordinating robots. However, our work is also more broadly applicable to any domain that would benefit from sparsifying the discrete latent distribution of a pre-trained CVAE. As such, in the process of sparsification, any inherent bias in the pre-trained network may be amplified, causing potential ethical concerns. Also, although we extensively validate our work empirically, we do not provide theoretical safety guarantees for the removed latent classes, requiring sufficient safety testing for any downstream task. We hope that our contribution will enable future positive research outcomes within the fields of robotics, generative modeling, and evidential theory.

Acknowledgments and Disclosure of Funding

We thank Tim Salzmann for helping us with the behavior prediction experiments. We thank Prof. Katherine Driggs-Campbell and Spencer M. Richards for their valuable feedback. We thank Dr. Boris Kirshtein for his advice and assistance. Toyota Research Institute (“TRI”) provided funds to assist the authors with their research but this article solely reflects the opinions and conclusions of its authors and not TRI or any other Toyota entity.

References

- [1] Yishu Miao and Phil Blunsom. Language as a latent variable: Discrete generative models for sentence compression. In *Conference on Empirical Methods in Natural Language Processing (EMNLP)*, pages 319–328, 2016.
- [2] Aaron van den Oord, Oriol Vinyals, and Koray Kavukcuoglu. Neural discrete representation learning. In *Advances in Neural Information Processing Systems (NeurIPS)*, pages 6306–6315, 2017.
- [3] Ali Razavi, Aaron van den Oord, and Oriol Vinyals. Generating diverse high-fidelity images with VQ-VAE-2. In *Advances in Neural Information Processing Systems (NeurIPS)*, pages 14837–14847, 2019.
- [4] Tim Salzmann, Boris Ivanovic, Punarjay Chakravarty, and Marco Pavone. Trajectron++: Dynamically-feasible trajectory forecasting with heterogeneous data. In *European Conference on Computer Vision (ECCV)*, 2020.
- [5] Edward Schmerling, Karen Leung, Wolf Vollprecht, and Marco Pavone. Multimodal probabilistic model-based planning for human-robot interaction. In *International Conference on Robotics and Automation (ICRA)*, pages 1–9. IEEE, 2018.
- [6] Thomas M Moerland, Joost Broekens, and Catholijn M Jonker. Learning multimodal transition dynamics for model-based reinforcement learning. In *29th Benelux Conference on Artificial Intelligence*, page 362, 2017.
- [7] Eric Jang, Shixiang Gu, and Ben Poole. Categorical reparameterization with Gumbel-Softmax. In *International Conference on Learning Representations (ICLR)*, 2017.
- [8] Boris Ivanovic and Marco Pavone. The Trajectron: Probabilistic multi-agent trajectory modeling with dynamic spatiotemporal graphs. In *International Conference on Computer Vision (ICCV)*. IEEE, 2019.
- [9] Rachit Singh. Sequential discrete latent variables for language modeling. Bachelor’s thesis, Harvard University, 2018.
- [10] Lukasz Kaiser, Samy Bengio, Aurko Roy, Ashish Vaswani, Niki Parmar, Jakob Uszkoreit, and Noam Shazeer. Fast decoding in sequence models using discrete latent variables. In *International Conference on Machine Learning (ICML)*, pages 2390–2399, 2018.
- [11] Arash Vahdat, William Macready, Zhengbing Bian, Amir Khoshaman, and Evgeny Andriyash. DVAE++: Discrete variational autoencoders with overlapping transformations. In *International Conference on Machine Learning (ICML)*, pages 5035–5044, 2018.
- [12] Brian Ichter, James Harrison, and Marco Pavone. Learning sampling distributions for robot motion planning. In *International Conference on Robotics and Automation (ICRA)*, pages 7087–7094. IEEE, 2018.
- [13] Sandeep Chinchali, Apoorva Sharma, James Harrison, Amine Elhafsi, Daniel Kang, Evgenya Pergament, Eyal Cidon, Sachin Katti, and Marco Pavone. Network offloading policies for cloud robotics: a learning-based approach. In *Robotics: Science and Systems (RSS)*, 2019.
- [14] Alex X. Lee, Richard Zhang, Frederik Ebert, Pieter Abbeel, Chelsea Finn, and Sergey Levine. Stochastic adversarial video prediction. *arXiv*, 2018.
- [15] Namhoon Lee, Wongun Choi, Paul Vernaza, Christopher B Choy, Philip HS Torr, and Manmohan Chandraker. DESIRE: Distant future prediction in dynamic scenes with interacting agents. In *Conference on Computer Vision and Pattern Recognition (CVPR)*, pages 336–345. IEEE, 2017.
- [16] Kihyuk Sohn, Honglak Lee, and Xinchen Yan. Learning structured output representation using deep conditional generative models. In *Advances in Neural Information Processing Systems (NeurIPS)*, pages 3483–3491, 2015.

- [17] Arthur P. Dempster. A generalization of Bayesian inference. *Classic works of the Dempster-Shafer Theory of Belief Functions*, pages 73–104, 2008.
- [18] Fabio Cuzzolin. Visions of a generalized probability theory. *arXiv*, 2018.
- [19] Thierry Denoeux. Logistic regression, neural networks and Dempster-Shafer theory: A new perspective. *Knowledge-Based Systems*, 2019.
- [20] Glenn Shafer. *A mathematical theory of evidence*, volume 42. Princeton University Press, 1976.
- [21] Thierry Denoeux. Introduction to belief functions. 4th School on Belief Functions and their Applications, 2017.
- [22] Barry R. Cobb and Prakash P. Shenoy. On the plausibility transformation method for translating belief function models to probability models. *International Journal of Approximate Reasoning*, 41(3):314–330, 2006.
- [23] Philippe Smets. Belief functions: the disjunctive rule of combination and the generalized Bayesian theorem. *International Journal of Approximate Reasoning*, 9(1):1–35, 1993.
- [24] Andre Martins and Ramon Astudillo. From softmax to sparsemax: A sparse model of attention and multi-label classification. In *International Conference on Machine Learning (ICML)*, pages 1614–1623, 2016.
- [25] Yann LeCun, Léon Bottou, Yoshua Bengio, and Patrick Haffner. Gradient-based learning applied to document recognition. *Proceedings of the IEEE*, 86(11):2278–2324, 1998.
- [26] Oriol Vinyals, Charles Blundell, Timothy Lillicrap, and Daan Wierstra. Matching networks for one shot learning. In *Advances in Neural Information Processing Systems (NeurIPS)*, pages 3630–3638, 2016.
- [27] Han Xiao, Kashif Rasul, and Roland Vollgraf. Fashion-MNIST: a novel image dataset for benchmarking machine learning algorithms. *arXiv*, 2017.
- [28] Yaroslav Bulatov. NotMNIST dataset. *Google (Books/OCR), Tech. Rep. [Online]. Available: <http://yaroslavvb.blogspot.it/2011/09/notmnist-dataset.html>*, 2, 2011.
- [29] Chris J. Maddison, Andriy Mnih, and Yee Whye Teh. The Concrete distribution: A continuous relaxation of discrete random variables. In *International Conference on Learning Representations (ICLR)*, 2017.
- [30] Jia Deng, Wei Dong, Richard Socher, Li-Jia Li, Kai Li, and Li Fei-Fei. ImageNet: A large-scale hierarchical image database. In *Conference on Computer Vision and Pattern Recognition (CVPR)*, pages 248–255. IEEE, 2009.
- [31] Aaron Van den Oord, Nal Kalchbrenner, Lasse Espeholt, Oriol Vinyals, Alex Graves, and Koray Kavukcuoglu. Conditional image generation with PixelCNN decoders. In *Advances in Neural Information Processing Systems (NeurIPS)*, pages 4790–4798, 2016.
- [32] Sergey Zagoruyko and Nikos Komodakis. Wide Residual Networks. In *Proceedings of the British Machine Vision Conference (BMVC)*, pages 87.1–87.12, 2016.
- [33] Irina Higgins, Loic Matthey, Arka Pal, Christopher Burgess, Xavier Glorot, Matthew Botvinick, Shakir Mohamed, and Alexander Lerchner. Beta-VAE: Learning basic visual concepts with a constrained variational framework. In *International Conference on Learning Representations (ICLR)*, volume 2, page 6, 2017.
- [34] Shengjia Zhao, Jiaming Song, and Stefano Ermon. InfoVAE: Balancing learning and inference in variational autoencoders. In *Conference on Artificial Intelligence. AAAI*, 2019.
- [35] Stefano Pellegrini, Andreas Ess, Konrad Schindler, and Luc Van Gool. You’ll never walk alone: Modeling social behavior for multi-target tracking. In *International Conference on Computer Vision (ICCV)*, pages 261–268. IEEE, 2009.

- [36] Emile Mathieu, Tom Rainforth, N Siddharth, and Yee Whye Teh. Disentangling disentanglement in variational autoencoders. In *International Conference on Machine Learning (ICML)*, pages 4402–4412, 2019.
- [37] Adam Kosioerek, Hyunjik Kim, Yee Whye Teh, and Ingmar Posner. Sequential attend, infer, repeat: Generative modelling of moving objects. In *Advances in Neural Information Processing Systems (NeurIPS)*, pages 8606–8616, 2018.
- [38] Murat Sensoy, Lance Kaplan, and Melih Kandemir. Evidential deep learning to quantify classification uncertainty. In *Advances in Neural Information Processing Systems (NeurIPS)*, pages 3179–3189, 2018.
- [39] Włodzisław Duch and Łukasz Itert. A posteriori corrections to classification methods. In *Neural Networks and Soft Computing*, pages 406–411. Springer, 2003.
- [40] Anirban Laha, Saneem Ahmed Chemmengath, Priyanka Agrawal, Mitesh Khapra, Karthik Sankaranarayanan, and Harish G Ramaswamy. On controllable sparse alternatives to softmax. In *Advances in Neural Information Processing Systems (NeurIPS)*, pages 6422–6432, 2018.
- [41] Gonçalo M Correia, Vlad Niculae, Wilker Aziz, and André FT Martins. Efficient marginalization of discrete and structured latent variables via sparsity. *arXiv*, 2020.
- [42] Diederik P. Kingma and Jimmy Ba. Adam: A method for stochastic optimization. In *International Conference on Learning Representations (ICLR)*, 2015.

A Evidential Theory

A.1 Supplementary Background

Evidential theory diverges from Bayesian probability theory by modifying Kolmogorov's definition of a probability measure [20], as follows:

Definition A.1. Given a finite set $Z = \{z_1, \dots, z_K\}$ and the power set 2^Z , the evidential belief function $Bel : 2^Z \rightarrow [0, 1]$ satisfies the following conditions:

1. $Bel(\emptyset) = 0$
2. $Bel(Z) = 1$
3. For every positive integer n and every collection A_1, \dots, A_n of subsets of Z ,

$$Bel(A_1 \cup A_n) \geq \sum_i Bel(A_i) - \sum_{i < j} Bel(A_i \cap A_j) + \dots + (-1)^{n+1} Bel(A_1 \cap \dots \cap A_n). \quad (11)$$

The conditions for an evidential belief function are identical to those in Bayesian theory, with the exception that the third condition is relaxed to a lower bound rather than an equality [20]. The evidential belief assigned to a set $A \subseteq Z$ as defined above includes the belief committed to any subset of A , as well. If we want to consider the belief assigned to exactly the set A , we use the concept of a basic probability assignment or a belief mass function [20], as follows:

Definition A.2. Given a finite set $Z = \{z_1, \dots, z_K\}$ and the power set 2^Z , the basic probability assignment or evidential belief mass function $m : 2^Z \rightarrow [0, 1]$ satisfies the following conditions:

1. $m(\emptyset) = 0$
2. $\sum_{A \subseteq Z} m(A) = 1$.

The belief function, which is also referred to as a *lower probability* of A , can also be expressed in terms of the mass function, as follows:

$$Bel(A) = \sum_{B \subseteq A} m(B). \quad (12)$$

In parallel, the *upper probability* of A , or the plausibility of A [20], is defined as follows:

$$Pl(A) = 1 - Bel(\bar{A}). \quad (13)$$

The existence of upper and lower probabilities differentiates evidential theory from Bayesian methods. Evidential theory is able to distinguish between lack of evidence towards a hypothesis and evidence against a hypothesis. Thus, the belief function indicates the total belief committed to the set A and its subsets [18], whereas plausibility is the amount of evidence *not* against A [18].

A.2 Illustrative Example

To provide better intuition for evidential theory, we outline an example here. Consider a region in space that may be occupied by an obstacle. Let z_1 correspond to the hypothesis that the region is *occupied*, z_2 to the hypothesis that the region is *free*, and $Z = \{z_1, z_2\}$. Then, we have $2^Z = \{\emptyset, \{z_1\}, \{z_2\}, Z\}$. The belief mass assigned to the set Z is an indication of uncertainty or lack of evidence. Thus, when there are no sensor measurements, we do not have any information, and can assign the entirety of the mass to the unknown set Z . Suppose, we then receive many conflicting measurements of whether the region is occupied or free (for instance due to moving obstacles entering and leaving the region). The mass from the uncertainty set Z will then move to the hypotheses $\{z_1\}$ and $\{z_2\}$, respectively. Hence, the belief will transition from lack of information to conflicting information. In the classic Bayesian counterpart scenario, we would have a uniform prior before a measurement is received, and we would approach the same probability mass distribution when equally many occupied and free sensor measurements are received. As illustrated by this example, evidential theory is able to distinguish lack of information from conflicting information.

A.3 Evidence Fusion

Two independent sources of evidence represented by belief masses can be combined through Dempster’s rule to generate a fused mass function as follows [17],

$$(m_1 \oplus m_2)(A) = \frac{1}{1 - \kappa} \sum_{B \cap C = A} m_1(B)m_2(C), \quad (14)$$

$$\forall A \subseteq Z, A \neq \emptyset \text{ and } (m_1 \oplus m_2)(\emptyset) = 0$$

where $\kappa = \sum_{B \cap C = \emptyset} m_1(B)m_2(C)$ is the degree of conflict between two belief mass functions. Two belief mass functions can be combined through Dempster’s rule only if for at least one pair $A \subseteq Z$ and $B \subseteq Z$, $m(A) \neq 0$, $m(B) \neq 0$, and $A \cap B \neq \emptyset$ [18]. Dempster’s rule reduces to Bayes’ rule in the special case of the combination of a vacuous mass function and a mass function with non-zero elements only over singleton sets [18].

B DST-Softmax Equivalence Satisfaction

The constraint required to ensure that the DST combination is equivalent to the softmax transformation is: $\sum_{j=1}^J \alpha_{jk} = \hat{\beta}_{0k} + c_0$ for some constant c_0 . Computing, we have:

$$\sum_{j=1}^J \alpha_{jk} = \sum_{j=1}^J \left[\frac{1}{J} \left(\beta_{0k} + \sum_{j=1}^J \beta_{jk} \phi_j(x_i) \right) - \beta_{jk} \phi_j(x_i) \right] \quad (15)$$

$$= \sum_{j=1}^J \frac{1}{J} \left(\beta_{0k} + \sum_{j=1}^J \beta_{jk} \phi_j(x_i) \right) - \sum_{j=1}^J \beta_{jk} \phi_j(x_i) \quad (16)$$

$$= \frac{1}{J} \left(\beta_{0k} + \sum_{j=1}^J \beta_{jk} \phi_j(x_i) \right) \sum_{j=1}^J 1 - \sum_{j=1}^J \beta_{jk} \phi_j(x_i) \quad (17)$$

$$= \frac{1}{J} \left(\beta_{0k} + \sum_{j=1}^J \beta_{jk} \phi_j(x_i) \right) J - \sum_{j=1}^J \beta_{jk} \phi_j(x_i) \quad (18)$$

$$= \left(\beta_{0k} + \sum_{j=1}^J \beta_{jk} \phi_j(x_i) \right) - \sum_{j=1}^J \beta_{jk} \phi_j(x_i) \quad (19)$$

$$= \beta_{0k} \quad (20)$$

$$= \hat{\beta}_{0k} - \frac{1}{K} \sum_{l=1}^K \hat{\beta}_{0l}. \quad (21)$$

The last line follows from the result in Eq. (8). Therefore, we have shown that the new α_{jk} parameters meet the required constraint for DST-softmax equivalence as posed by Denoeux [19].

C MNIST, Fashion MNIST, and NotMNIST Image Generation Experimental Details

We chose the following class reassignment scheme for Fashion MNIST: *tops* and *bottoms/accessories*. For the MNIST and Fashion MNIST experiments, we use a hidden unit dimensionality of 30 for $p(z | y)$ and 256 for $p(z | x, y)$ and $p(x' | z)$ within the architecture in Fig. 1. We chose the 256 dimension following the example from: <https://github.com/timbmg/VAE-CVAE-MNIST>. We use the ReLU nonlinearity with stochastic gradient descent and Adam [42] optimizers and a learning rate of 0.001 for the MNIST [25] and Fashion MNIST [27] datasets respectively. We train for 20 epochs with a batch size of 64.

To investigate a similar image generation task on a more complicated dataset, we consider the NotMNIST benchmark, which requires a more expressive architecture. We consider the task of

generating letters with and without a horizontal bar in the center. The convolutional architecture for the NotMNIST experiments is depicted in Fig. 5. Similar to the network for (Fashion) MNIST, during training, the encoder consists of two network blocks. One fully-connected block takes as input the query label y , and outputs a softmax probability distribution that parameterizes the prior distribution $p(z | y)$, where z is a discrete latent variable that can take on K values. The second block takes as input the stacked feature vector x and query label y , and outputs the softmax distribution for the posterior $q(z | x, y)$ after a series of convolutional layers. The z value is sampled from the posterior distribution q during training and the prior distribution p at test time. It is then passed through the decoder convolutional network block to predict the image output x' . As before, the Gumbel-Softmax distribution is used to backpropagate loss gradients through the discrete latent space [7, 29]. We use the ReLU nonlinearity with the stochastic gradient descent optimizer and a learning rate of 0.00001. We train for 1000 epochs with a batch size of 256.

For the MNIST, FashionMNIST, and NotMNIST experiments, the standard conditional evidence lower bound (ELBO) was maximized to train the model [16]:

$$\mathcal{L}(x, y; \theta) = \mathbb{E}[\log(p_D(x | z; \theta))] - \text{KL}[q(z | x, y; \theta) || p(z | y; \theta)], \quad (22)$$

where p_D is the distribution output by the decoder and θ are the network parameters.

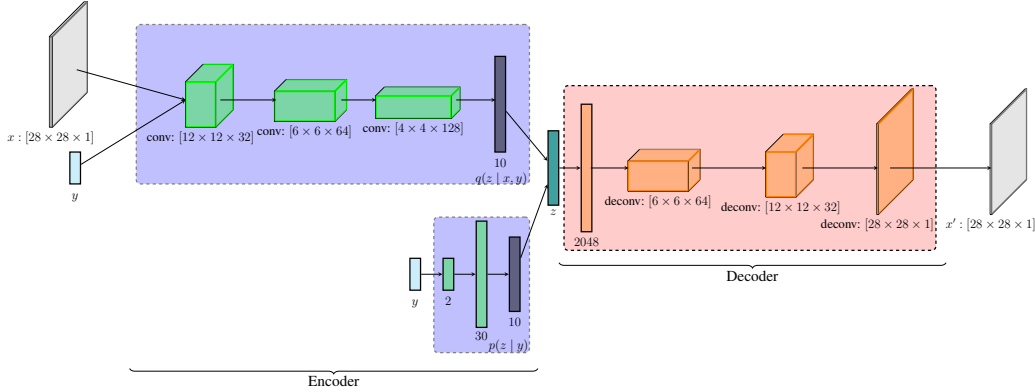


Figure 5: The CVAE architecture used for NotMNIST image generation. The last layer in each encoder network block is the softmax layer. At test time, $p(z | y)$ is used to sample the latent space; thus, only the input query y serves as input to the encoder.

D MNIST CVAE Test-Time Performance Comparison

Fig. 6 shows a comparison of the generated images sampled from the softmax discrete latent distribution versus our proposed filtered distribution for the *even* input query. The softmax distribution often samples visually incorrect latent classes given the *even* input query. Our method improves the test time sampling performance of the CVAE by pruning the majority of the erroneous latent classes, while keeping the correct ones. When considering 25 samples for the *even* input, softmax produces eight incorrect samples, while our method produces only three (the incorrect 9 image).

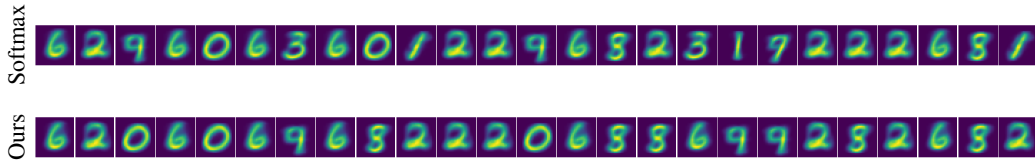


Figure 6: Samples from the CVAE at test time for the *even* input using the softmax distribution and our proposed distribution. Our distribution results in samples that are more accurate with the exception of the sampled 9 digit. The filtered *even* distribution no longer includes the incorrect latent classes for the 1 and 3 digits.

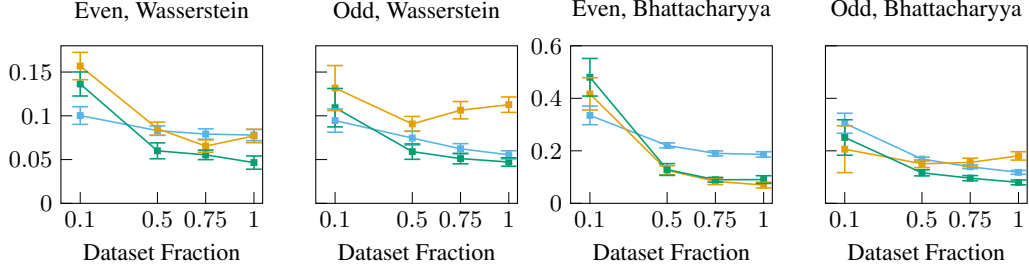


Figure 7: Our proposed distribution (green) extracts more accurate information across fewer training examples on the MNIST dataset as compared to the softmax (blue) and sparsemax (orange) baselines. Lower is better for the distance metrics. The results are over 25 different random seeds.

E Reduced Data Performance for MNIST

We investigate whether evidential latent space sparsification is able to extract more accurate information than softmax and sparsemax when the learned model is hindered by a smaller training set. Fig. 7 summarizes the performance of the proposed filtered distribution for a network trained on a reduced MNIST dataset. We use 0.1, 0.5, 0.75, and 1.0 fractions of the dataset for training, maintaining the class balance and evaluating after 20 training epochs. The filtered distribution largely outperforms softmax outside of standard error across both metrics on the MNIST dataset. Our method also outperforms the sparsemax baseline when the latter is hindered by its generation of false negative latent classes (e.g., for the *odd* input query).

F Results on Fashion MNIST

F.1 Qualitative Results

We investigate the qualitative performance of our proposed methodology on the Fashion MNIST dataset. The network learns a more accurate softmax distribution than that for the MNIST dataset as shown in Fig. 8. The more effective softmax distribution learned for the Fashion MNIST dataset than that for MNIST is likely due to the more distinct features across the dataset’s categories. Nevertheless, our filtered distribution still provides further improvement for the latent class distribution by filtering out incorrect probability masses completely. We note that the filtered distribution makes two mistakes in keeping the first latent class (a boot) for the *tops* input query and keeping the sixth latent class (a shirt) for the *bottoms* input query. Nevertheless, we emphasize that these are false positives. As with MNIST, sparsemax results in aggressive filtering that removes valid latent classes for each query, such as the dress from the *tops* category, and a boot as well as two purses from the accessories

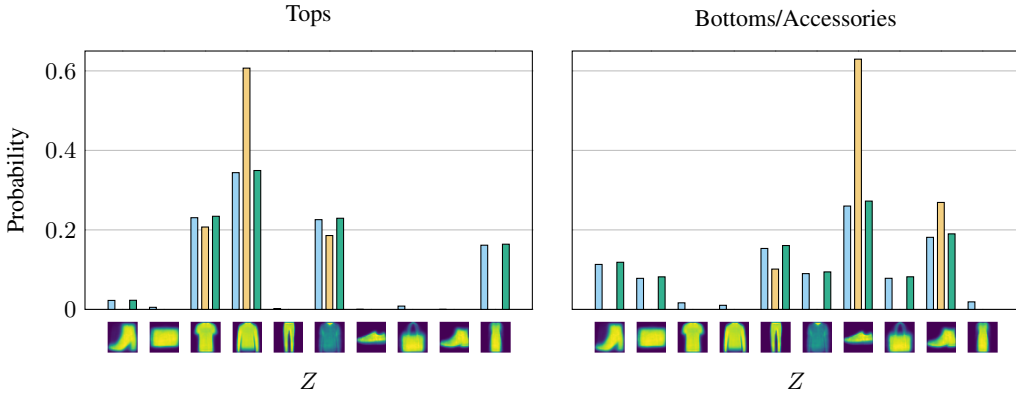


Figure 8: Our proposed filtered distribution (green) is compared to the softmax (blue) and sparsemax (orange) distributions on the Fashion MNIST dataset. The horizontal axis depicts decoded latent classes. Our method reduces the size of the relevant latent sample space without removing valid latent classes.

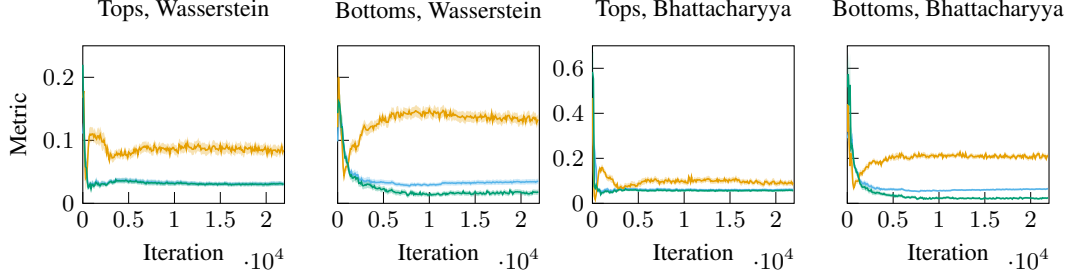


Figure 9: Our filtered distribution (green) outperforms the softmax (blue) and sparsemax (orange) baselines across training iterations on the Fashion MNIST dataset. Lower is better for distance metrics. The results are over 25 different random seeds.

category. Qualitatively, our filtered distribution outperforms the baselines on the Fashion MNIST dataset, providing a sparser, more accurate distribution than softmax, while avoiding false negatives, which would be undesirable for safety critical applications.

F.2 Training Evolution Results

Fig. 9 shows that when the underlying network learns the latent space successfully, as is the case for Fashion MNIST data, our filtered distribution performs no worse (and even slightly better) than the original softmax distribution. The sparsemax distribution once again filters out valid latent classes from both binary queries, resulting in poor performance across our metrics. Thus, for the Fashion MNIST benchmark dataset, the proposed latent class distribution provides a more robust representation, retrieving richer information from the learned neural network weights with fewer training iterations.

F.3 Reduced Data Performance for Fashion MNIST

Fig. 10 summarizes the performance of the filtered distribution on a network trained on a reduced Fashion MNIST dataset. Due to the more effectively learned encoder weights, our filtered distribution maintains the performance of the original softmax distribution. Our proposed distribution significantly outperforms the sparsemax baseline due to the aggressive sparsemax filtering that results in false negatives. Sparsemax continues to select a subset of more likely encodings, at the cost of removing valid latent classes, making it undesirable for applications where false negatives are safety critical. We note that the difference between the Wasserstein and Bhattacharyya metrics in Fig. 10 are due to the latter favoring sparse distributions by definition.

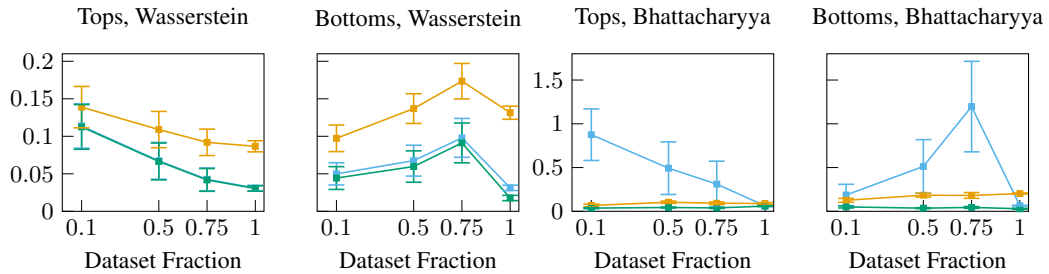


Figure 10: Filtered distribution performance across fewer training samples on the Fashion MNIST dataset. Our filtered distribution (green) demonstrates more robust performance than the softmax (blue) and sparsemax (orange) on our metrics. The results are over 25 different random seeds.

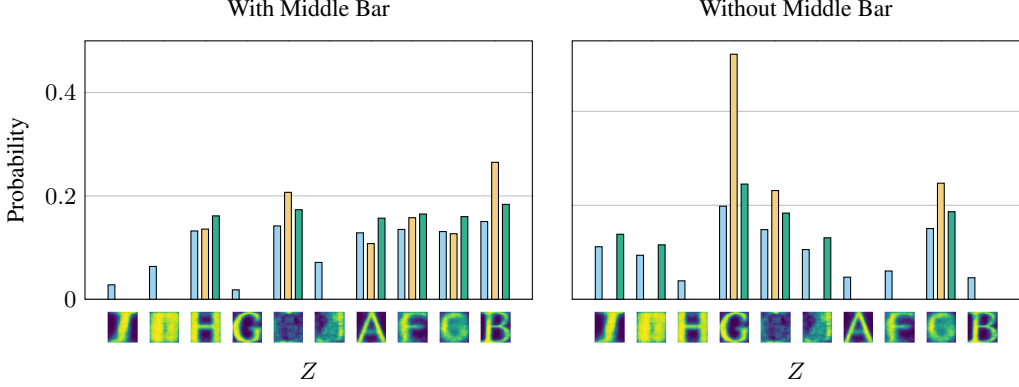


Figure 11: Our proposed filtered distribution (green) is compared to the softmax (blue) and sparsemax (orange) distributions on the NotMNIST dataset. The horizontal axis depicts decoded latent classes. Our method reduces the size of the relevant latent sample space without removing valid latent classes.

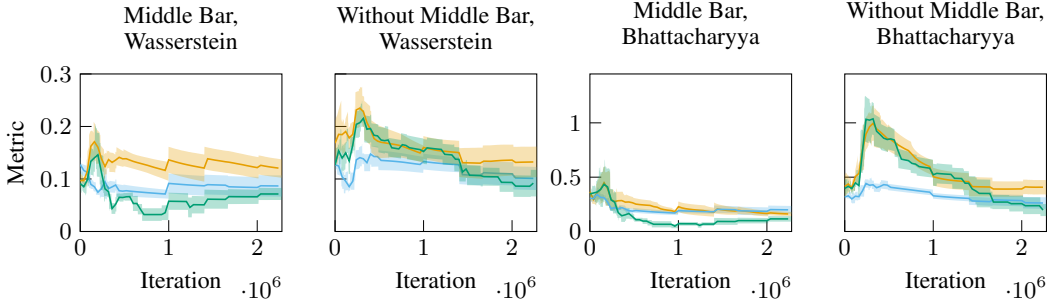


Figure 12: Our filtered distribution (green) outperforms sparsemax (orange) and softmax (blue) over training iterations when the network weights have been trained sufficiently on the NotMNIST dataset. Lower is better for distance metrics. The results are over 5 different random seeds.

G NotMNIST Image Generation Results

G.1 Qualitative Performance

Fig. 11 shows a comparison of our proposed method, the original softmax distribution, and sparsemax for the *with middle bar* and *no middle bar* letter queries on the NotMNIST dataset. Once again, although the CVAE architecture proposed in Fig. 5 successfully learns a multimodal latent encoding, the learned softmax probability distribution has non-negligible probability masses associated with the incorrect latent classes z_k for each query class y .

We observe that our filtered distribution selects a plausible set of correct latent classes given an input query as shown in Fig. 11. Since NotMNIST is a more difficult dataset, the decoded latent classes are, at times, an unrecognizable combination of features which scores high for both input queries. Outside of these cases, we successfully sparsify the latent space analytically for each query class without knowledge of or comparison to the other query. As before, sparsemax continues to generate excessive false negatives, for instance, filtering out the ‘I’ for the *without middle bar* query. Thus, our more conservative, yet effective, filtration is a compelling latent space reduction technique.

G.2 Quantitative Performance

Training Evolution Fig. 12 shows the performance of our filtered distribution on the NotMNIST dataset at different training iterations. For the *with middle bar* input query, we continue to demonstrate the robustness of our filtered distribution to fewer training iterations. Our method extracts more accurate encoding information from the neural network earlier in the training process than the softmax and sparsemax baselines. However, we note that both our filtered distribution and sparsemax

underperform the softmax baseline at the beginning of training for the *without middle bar* query. Since the NotMNIST dataset is substantially bigger and more difficult than (Fashion) MNIST, the neural network weights governing the latent distribution can take longer to become meaningful. Hence, we observed that for these early iterations, it is not possible for a method with an implicit threshold, such as our filtration or sparsemax, to accurately filter the distribution. As in other experiments, our filtered distribution can only perform as well as the learned network. However, our distribution continues to consistently outperform sparsemax due to the latter’s aggressive filtration which incorrectly filters out potentially valid latent classes.

H VQ-VAE Experimental Details

We train the VQ-VAE [2] network on *miniImageNet* [26] data randomly cropped to 128×128 and normalized to $[-1, 1]$. The *miniImageNet* dataset consists of 38,400 examples in the training set, 9,600 in the validation set, and 12,000 in the test set. *miniImageNet* was designed for few-shot learning tasks, thus the classes do not overlap between the dataset splits. There are 64 classes in the training set. We use *miniImageNet* to test the algorithm due to its more computationally feasible size for training on a single NVIDIA GeForce GTX 1070 GPU. We train the VQ-VAE with the default parameters from: <https://github.com/ritheshkumar95/pytorch-vqvae>. We use a batch size of 128 for 100 epochs, $K = 512$ for the number of classes for each of the 32×32 latent variables, a hidden size of 256, and a β of one. The network was trained with the Adam optimizer and a starting learning rate of 2×10^{-4} . We use the best model according to the validation loss. To sanity check that the VQ-VAE latent space reasonably captures the data, we demonstrate example input and output images from the *miniImageNet* test set in Fig. 13. Since *miniImageNet* is meant for one-shot learning, the classes in the training set do not match those in the validation and test sets. Thus, the data distribution in the test set is different than that of the training set. The trained VQ-VAE is able to reasonably reconstruct these out-of-distribution images. We then train the PixelCNN [31] prior over the latent space with 20 layers, hidden dimension of 128, a batch size of 32 for 100 epochs. The network was trained with the Adam optimizer and a starting learning rate of 3×10^{-4} .

We generate a new dataset by sampling from the trained prior, and decoding the images using the VQ-VAE decoder. We sample 25 latent encodings from the prior for each of the 64 *miniImageNet* training classes to build the dataset. We perform the sampling using the original softmax, sparsemax, and our proposed latent distributions. We extract equivalent linear layer weights and biases for the last 1D convolutional layer in PixelCNN to pass as input to our proposed distribution and sparsemax. Examples of the sampled images are shown below in Fig. 14. Our proposed sparse latent distribution visually maintains the same performance as the softmax distribution. Images sampled using the sparsemax distribution are not depicted as they degenerate to single color blocks due to sparsemax severely collapsing the distributional multimodality in the PixelCNN prior.

We then train a Wide Residual Network (WRN) [32] for classification on *miniImageNet*. We use the PyTorch implementation for WRN found here: <https://pytorch.org/docs/stable/torchvision/models.html> and the training protocol proposed here: https://github.com/huyvnphan/PyTorch_CIFAR10. We train WRN on a subset of the *miniImageNet* training set, leaving 5% out for validation. WRN is trained for 100 epochs with a batch size of 128. The optimizer is stochastic gradient descent with a learning rate of 1×10^{-2} . The inference performance of the WRN classifier on the datasets generated with the softmax, sparsemax, and our proposed latent distributions are compared, demonstrating that our distribution, unlike sparsemax, is able to maintain the performance of softmax, while significantly reducing the size of the latent sample space.

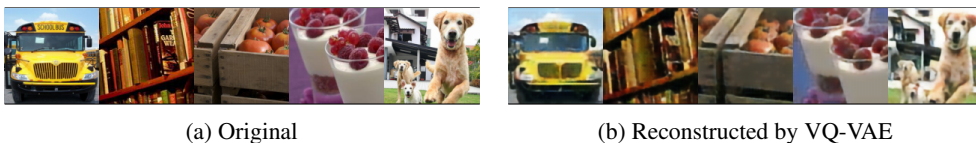


Figure 13: Images are reconstructed using VQ-VAE from the test set of *miniImageNet*.

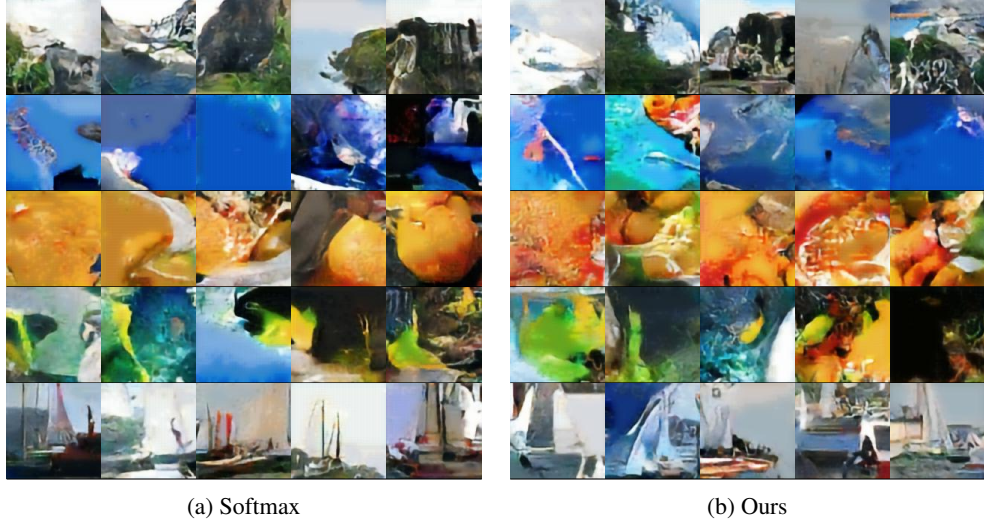


Figure 14: Images are generated for the queries (top to bottom): “cliff”, “jellyfish”, “orange”, “rock beauty”, and “yaw!” using the original softmax and our proposed latent distributions. Both sets of sampled images are of similar quality despite our distribution considering a much smaller latent sample space. Images sampled using sparsemax are not depicted as they degenerate to solid color blocks due to sparsemax collapsing the multimodality in the autoregressive latent space distribution.

I Behavior Prediction Experimental Details

Fig. 15 illustrates the architecture of the Trajectron++ network with internal layer sizes for reference, as depicted in Salzmann et al. [4]. The model was trained for 2000 iterations with a batch size of 256 and an initial learning rate of 1×10^{-3} which was exponentially annealed down to 1×10^{-5} with a decay rate of 0.9999. The model was trained to predict 12 timesteps (4.8 s) into the future from 8 timesteps (3.2 s) of history. The loss function β weight was varied following a sigmoid function from 0 to 2.5 with the middle value achieved at 400 iterations. The model’s latent variables \mathbf{z} are one-hot categorical latent variables which are approximated with a Gumbel-Softmax distribution, enabling backpropagation through samples with the reparameterization trick [7]. The Gumbel-Softmax distribution’s temperature τ was exponentially annealed from 2.0 to 0.05 with a decay rate of 0.997. The decoder outputs Gaussian Mixture Model (GMM) means and covariances for each prediction timestep, where each GMM has 16 components. Our experiments were run on 50 randomly-sampled scenes from the ETH test dataset, within which there were 203 agent trajectories.

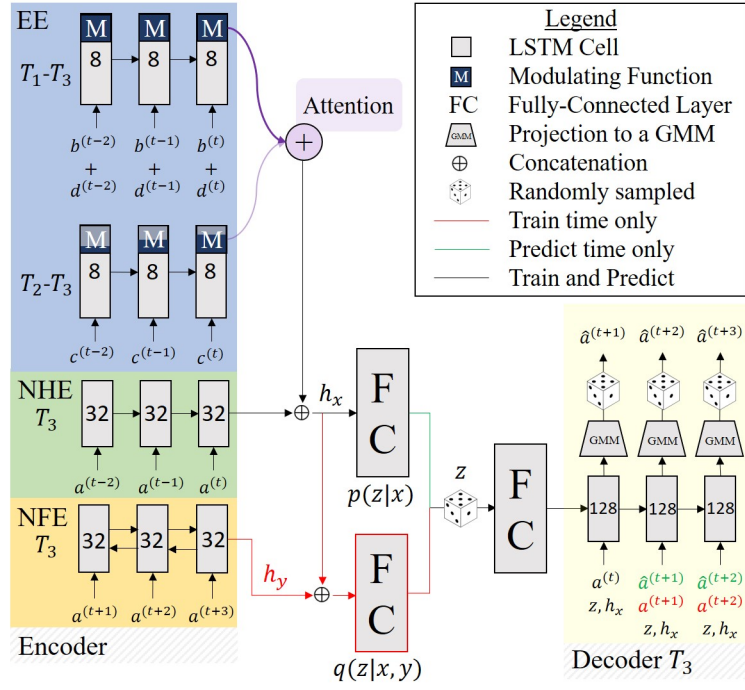


Figure 15: Trajectron++ architecture with layer dimensions indicated.